In Press, Accepted Manuscript – Note to user

Structural characterization and electrochemical performance of nitrogen doped graphene supercapacitor electrode fabricated by hydrothermal method

Mohd Asyadi Azam[1*], Nur Ezyanie Safie[1], Mohd Fareezuan Abdul Aziz[1,2], Raja Noor Amalina Raja Seman[1], Muhamad Rafi Suhaili[1], Anas Abdul Latiff[3], Faiz Arith[3], Anuar Mohamed Kassim[4], and Mohd Hanafi Ani[5]

[1]Fakulti Kejuruteraan Pembuatan, Universiti Teknikal Malaysia Melaka, Hang Tuah Jaya, 76100 Durian Tunggal, Melaka, Malaysia
[2]Centre for Research and Innovation Management, Universiti Teknikal Malaysia Melaka, Hang Tuah Jaya, 76100 Durian Tunggal, Melaka, Malaysia
[3]Fakulti Kejuruteraan Elektronik dan Kejuruteraan Komputer, Universiti Teknikal Malaysia Melaka, Hang Tuah Jaya, 76100 Durian Tunggal, Melaka, Malaysia
[4]Fakulti Kejuruteraan Elektrik, Universiti Teknikal Malaysia Melaka, Hang Tuah Jaya, 76100 Durian Tunggal, Melaka, Malaysia
[5]Faculty of Engineering, International Islamic University Malaysia, 50728 Kuala Lumpur, Malaysia

ABSTRACT

The introduction of nitrogen (N) into graphene is of great focus as it escalates overall device performance as the introduction of N atoms improves the electronics of the graphene. In this work, the N-doped graphene electrode was prepared by using a hydrothermal method where graphene nanoplatelet was used as active material and aqueous ammonia as the nitrogen source. The electrode was then used as the supercapacitor electrode. From Raman analysis, the I_D/I_G ratio of N-doped graphene has a higher value than that of pristine graphene. This indicates the N-doped graphene possessed more defects and has a higher degree of disorder within the graphene sheet. For X-ray diffraction analysis, the result exhibits a broad peak at $2\theta = 26.3°$, corresponding to the graphitic profile with an interlayer spacing of 3.57 Å. X-ray photoelectron spectroscopy analysis proved that there is a presence of nitrogen on the graphene surface, with 2.35 % of the atomic concentration. From the cyclic voltammetry, all curves showed an almost rectangular shape at the scan rates of 10 to 100 mVs^{-1}. The calculated specific gravimetric capacitance is 25.2 F g^{-1} at 10 mV s^{-1}. In addition, charge-discharge analysis confirmed the typical behavior of electric double layer capacitor from the linear symmetric slopes.

Keywords: graphene, hydrothermal method, nitrogen doped, supercapacitor

1. INTRODUCTION

Among all energy storage devices, the supercapacitors are known to rely on physical electrochemical processes, which consuming relative energy and power densities [1-4]. Supercapacitors have turned into a hot territory of research, to some extent since it can be charged quickly and convey severe blasts of energy. Furthermore, the supercapacitors are also being used in a large scale of energy applications. Electric double-layer capacitance (EDLC) is one type of supercapacitor that has very high capacitance with low applied voltage [5-7]. EDLC as the most favourable supercapacitor compared to others, in general is designed with symmetric electrodes composed of carbon nanomaterials including carbon nanotube and graphene [5].

Graphene is an atomic-scale honeycomb lattice and two-dimensional carbon composed of sp^2 hybridized carbons with great properties such as excellent thermal conductivity, large surface area, high chemical stability [8-11]. In graphene, carbon atoms are arranged in a hexagonal pattern with a single layer of carbon called graphene sheet [12-15]. Graphene normally has a band gap of zero, which is related to its massless electrons; however, its electrical conductivity is hard to alter [16-18]. Such a bandgap can be altered by surface modification or chemical doping. In theory, the doping method can modulate the bandgap that leads to interesting properties for many applications [19-20]. Various techniques are possible for the preparation of nitrogen (N)-doped graphene including direct synthesis and post-treatment [21-26].

Mainly, N-doping regulates the properties of carbon materials due to the similar atomic size and the availability of five valence electrons for the formation of strong valence bonds with carbon [27, 28]. The necessary bonding configurations within the carbon lattice, such as pyridinic-N, pyrrolic-N, and quaternary-N (or graphitic-N) were observed when nitrogen doped into graphene [29-31]. Pyridinic-N and pyrrolic-N are considered as dominant in N-doped graphene samples due to the theoretical prediction that at the edges of graphene lattice where N atoms are more thermodynamically stable [32]. Strong valence bonds may be formed by the graphene p-electronic system and the lone pair of the N atoms [33]. In addition, N-doping is efficient to improve the capacitance of the graphene electrode due to extra redox between electrolyte ions and carbon atoms [34-37]. The supercapacitor's capacitances as independent energy storage device is still not high enough for many applications and thus it only acts as supplement to batteries. This supercapacitor type has similar capabilities to those of pseudocapacitors, but still uses robust charging mechanisms and has superior performance in the life cycle [38].

In this work, the N-doped graphene electrode was fabricated from hydrothermal method for the use in supercapacitor and various characterization techniques have been used to observe the structural properties of the samples as well as the electrochemical characteristics of the device.

2. MATERIAL AND METHODS

2.1 Preparation of N-doped graphene electrode

The hydrothermal method employing aqueous ammonia (Sigma Aldrich) and deionized water was used to dope the nitrogen (N) onto the graphene surfaces. The Teflon-lined autoclave has been used to perform such hydrothermal treatment. First, 50 mg of graphene nanoplatelets (Terra Techno, USA) were dissolved in deionized water and sonicated for an hour. The mixture's pH level was adjusted to the range of 10.0 to 11.0 by adding ammonia solution and stirred for 10 minutes. After that, the mixture was transferred into the Teflon-lined autoclave and treated with hydrothermal for 12 hours at 130 °C. After cooled at room temperature, the mixture was filtered and washed with deionized water before being vacuum-dried in an oven for 3 hours at 80 °C. Electrode preparation began by mixing the fixed amount of N-doped graphene, super-P carbon (TIMCAL), and polytetrafluoroethylene (PTFE; Sigma Aldrich) binder with the weight ratio of 80:10:10. All these materials were grounded in the agate mortar in 5 minutes' time and mixed with N-Methyl-2-pyrrolidone (NMP) to produce the slurry. Then the slurry is uniformly pasted on the nickel foam (current collector) and pressed by using the 10-ton pressing machine. Lastly, the electrode was dried in vacuum oven for 10 hours at 80 °C.

2.2 Materials and electrode characterization

Raman analysis was using a spectroscopy (UniRAM-5300) with 532 nm (Nd:YAG) laser where the Raman shift was recorded between 200 cm^{-1} to 3200 cm^{-1} for the quality information. X-ray diffraction (XRD) analysis was done using a Bruker PANanalytical diffractometer with CuKα radiation λ = 0.15406 nm (k=1.5406 Å) to study the crystalline structure and phase composition of the electrode. X-ray photoelectron spectroscopy (XPS; ULVAC-PHI Quantera II) was conducted to examine the doping effect of nitrogen onto the graphene nanoplatelet surfaces. The wide (survey) and narrow scans were performed with Al Kα as the excitation source and the binding energies were calibrated using C1s and N1s peaks at 285.0 eV and 400.0 eV, respectively.

2.3 Electrochemical performance analyses

Cyclic voltammetry (CV) is a performance indicator to measure the current under the applied voltage condition. CV was also performed by computing the resulting current and cycling the electrode potential. Galvanostatic charge-discharge (GCD) is a technique to analyse the cyclic behaviour (charging and discharging process) of the supercapacitor. All measurements were performed using a workstation (WonAtech3000), and the symmetric supercapacitor was measured by using CR2032 type coin cell with 6 M of potassium hydroxide (KOH) electrolyte in a two-electrode cell system. The potential voltage window was set at 0.0 - 0.60 V due to the aqueous electrolyte usage. And, the average mass of active material was 9.54 mg.

3. RESULTS AND DISCUSSION

3.1 Raman analysis

The Raman spectra of pristine graphene nanoplatelet and nitrogen (N)-doped graphene or NG are shown in Figure 1. The estimation of the defects in graphene surface is the ratio of D and G bands' intensities. The lower value of I_D/I_G depicts a small number of structural defects present in the material/sample [39]. The pristine graphene nanoplatelet shows two typical peaks at 1337 cm^{-1} and 1563 cm^{-1}, designated as D and G bands, respectively (Figure 1 (a)). The D-band reveals the presence of defects in the graphitic lattice. Meanwhile, the G-band is known as a representative of carbon-carbon graphitic structure. The I_D/I_G ratio of pristine graphene was calculated to be 0.922.

Figure 1(b) shows the Raman spectrum of the NG sample. The D- and G-band of Raman shift for NG is 1342 cm^{-1} and 1570 cm^{-1}, respectively. The I_D/I_G ratio calculated for NG is 0.946. Similarly, the increase in I_D/I_G ratio from 0.922 to 0.946 indicates that defects are increased due to the introduction of nitrogen atoms into the graphene lattice. The decreasing of the G-band peak intensity in NG is due to the capability of nitrogen that is heteroatoms in electron-donating [40].
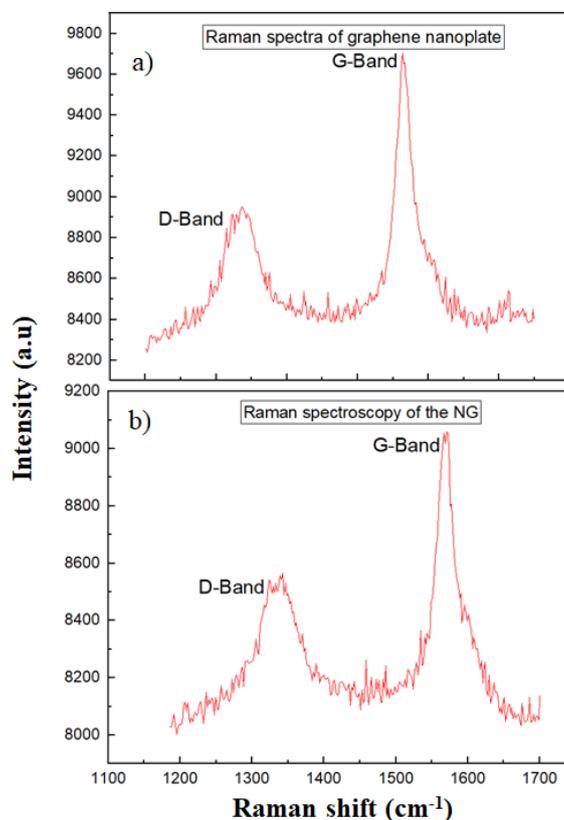
Figure 1. Raman analysis of a) pristine graphene nanoplatelet and b) N-doped graphene.

3.2 X-ray diffraction (XRD) analysis of N-doped graphene

The XRD patterns of N-doped graphene shown in Figure 2 confirms a reflection of peak (002) which located at 26.3°, where corresponds to d-spacing of 3.338 Å and a weak peak diffraction at 43.0° corresponds to peak (004). The appearance of a relatively broad peak at 26.3° confirmed that there is a possible formation of multiple layers of graphene because of the graphene reduction [41, 42].
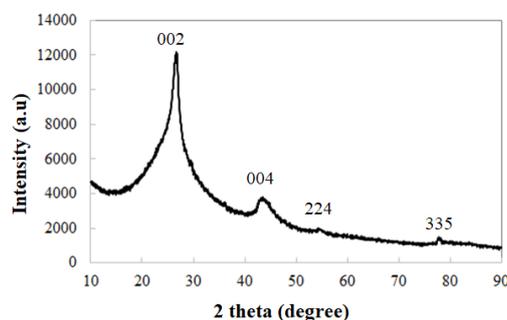
Figure 2. The XRD pattern of N-doped Graphene.

3.3 X-ray photoelectron spectroscopy (XPS) analysis just after sample preparation

Figure 3 shows XPS survey and narrow scans for N-doped graphene before electrochemical testing. There are 3 peaks at around 284.6 eV, 530 eV, and 400 eV that correspond to the existence of a graphitic C1s, a weak O1s, and a pronounced N1s, respectively (Figure 3a). XPS of C1s ranging from 280–290 eV (Figure 3b) and for N1s is at 398-403 eV (Figure 3c). The calculation by XPS elemental analysis shows the atomic concentration percentage of nitrogen that doped into the graphene is 2.35 %. In general, carbon contamination is commonly used as a charge reference for XPS spectra. C1s spectrum for this electrode typically has C-C, C-O, C-N, and O-C=O components. The C-C component may be set to a binding energy of 284.8eV, by default. The high resolution XPS of N1s spectrum of the N-doped graphene reveals 2 different types of nitrogen doping which is pyridinic-N and pyrrolic-N located at 399.1 and 400.7 eV, respectively. Pyridinic- and pyrrolic-N are dominant in N-doped graphene samples, confirming that nitrogen atoms are more stable at the graphene edges [43].
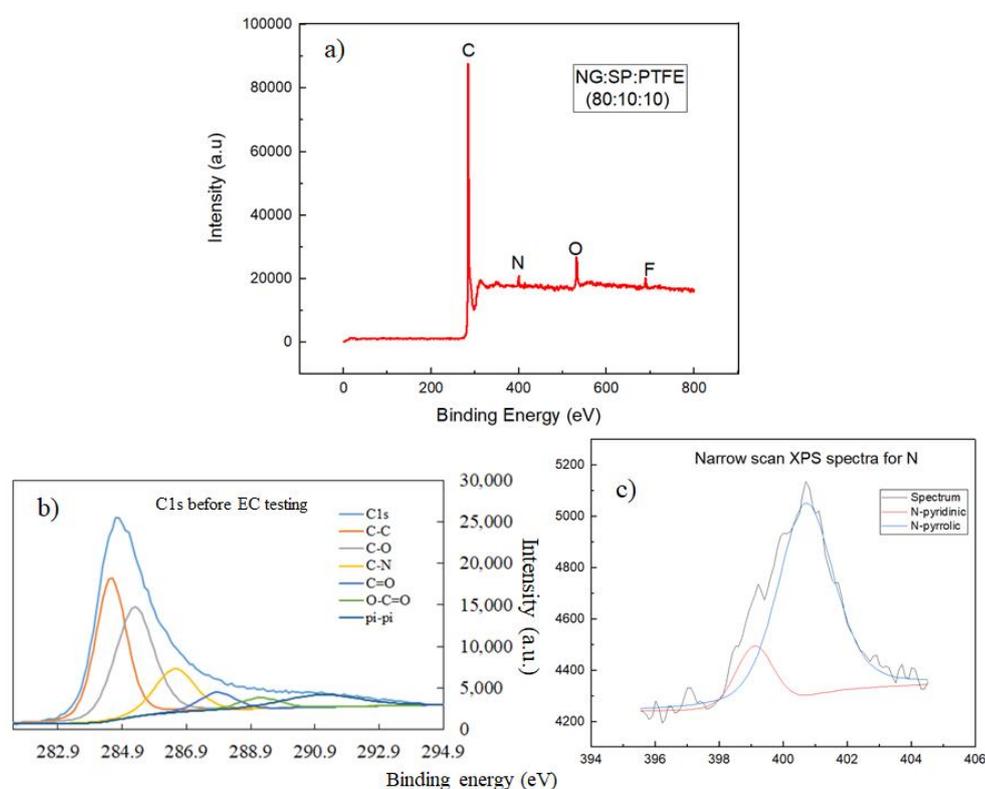

Figure 3. XPS analyses of the sample before electrochemical testing. a) Survey spectrum, b) narrow scan for C1s area, and c) narrow scan for N1s area.

3.4 Electrochemical performance analysis

With aim to understand the capacitive behaviour of N-doped graphene, CV and GCD measurements were conducted. CV curves of N-doped graphene at 0.0-0.6 V with the scan rate of 10, 50, 60, 80, 100, 200, 500 and 1000 mV s^{-1} are presented in Figure 4. Even at a fast scan rate of 100 mV s^{-1}, all CV curves exhibit shapes with a quasi-rectangular characteristic, suggesting a strong electrical double-layer capacitance (EDLC) behaviour (Figure 4(a)) [5].

Meanwhile, the CV curves showing leaf-type curves (less rectangular) at 200, 500 and 1000 mV s^{-1}. As the amount of scan rates increases, the area under the curve also increases. The virtually rectangular CV curves indicate the ideal and reversible capacitive behaviour of N-doped graphene electrode [44]. The current sustained by N-doped graphene is significantly high suggesting the enhanced electrochemical activity of N-doped graphene. The CV curve not showing a rectangular shape at high scan rates may be attributed from the fast physical separation occurred at the surfaces of the N-doped graphene [45].
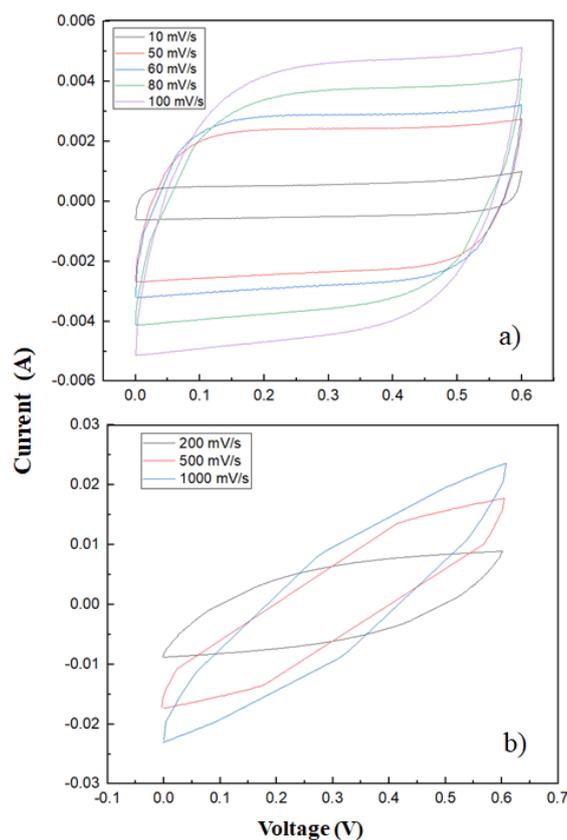

Figure 4. a) CV analysis for scan rate between 10-100 mV s^{-1}; b) CV analysis for scan rate between 200-1000 mV s^{-1}.

Figure 5(a) shows CV curve of N-doped graphene supercapacitor at 10 mV s^{-1}, in which the area of the curve is equivalent to the specific gravimetric capacitance (C_{sp}) and calculated by using the following equation [39]:

$$C_{sp} = \int_{E1}^{E2} i\ (E)dE \div (E2 - E1)mv \qquad (1)$$

E1 and E2 are the cut-off potentials, i(E) is the current, $\int_{E1}^{E2} i(E)dE$ is the total voltammetric charge in CV, m is the average mass, and v is the scan rate. The correlation between C_{sp} and the scan rates for N-doped graphene electrode is presented in Figure 5(b). The C_{sp} value was calculated to be 25.2 F g^{-1} at 10 mV s^{-1}. The C_{sp} values are decreasing with increasing scan rates. This suggests that at low scan rates, the active material takes enough time to participate in the chemical reaction that may occur at the electrode surface and the electrolyte ions [46].
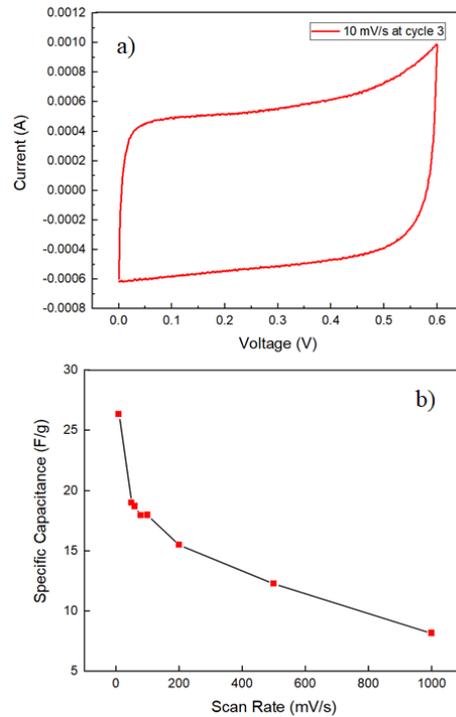
Figure 5. a) CV analysis for scan rate of 10 mV s^{-1} at third cycle and b) Specific capacitance for NG electrode for scan rates between 10-1000 mV s^{-1}.

In addition, Figure 6 presents the GCD curves of N-doped graphene supercapacitor in 6 M KOH electrolyte at the current of 1.5 mA or equivalent to 0.16 A g^{-1}. At 0.6 V, the anodic charges are typically symmetric to their cathodic discharging counterparts, revealing high capacitive reversibility without any voltage (IR) drop in N-doped graphene.
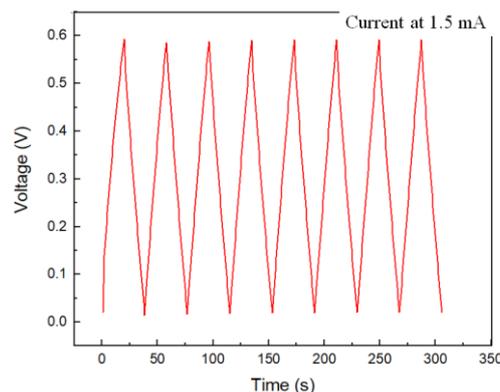

Figure 6. Charge discharge curve of N-doped graphene electrode.

3.5   XPS analysis of N-doped graphene after electrochemical testing

Figure 7 shows XPS survey and narrow scans for N-doped graphene after electrochemical performance testing. Six major peaks were observed from the wide scan of N-doped graphene

and this includes carbon (C), potassium (K1 and K2), nitrogen (N), oxygen (O) and fluoride (F) which located at 284, 292, 376, 400, 531, and 699 eV, respectively (Figure 7 a)). Similar to Figure 3b in Section 3.2, C1s spectrum for this electrode typically has C-C, C-O, C-N, and O-C=O components. However, the peak for C1s 2p3/2 core level was enhanced due to the formation of diamond or diamond like carbon. Further, this contribution gives one single carbon contribution at higher binding energy in agreement with the formation of diamond islands [47]. From Figure 7 c), 2 bonding configurations were observed; pyridinic-N and pyrrolic-N, which positioned at 398.76 and 400.50 eV, respectively. From these results, the percentage of atomic concentration of nitrogen after the electrochemical performance is decreasing to 0.98 %. This could be due to the disappearance of nitrogen atoms after such chemical reaction with the electrolyte, and also could be the formation to the other molecules [48].
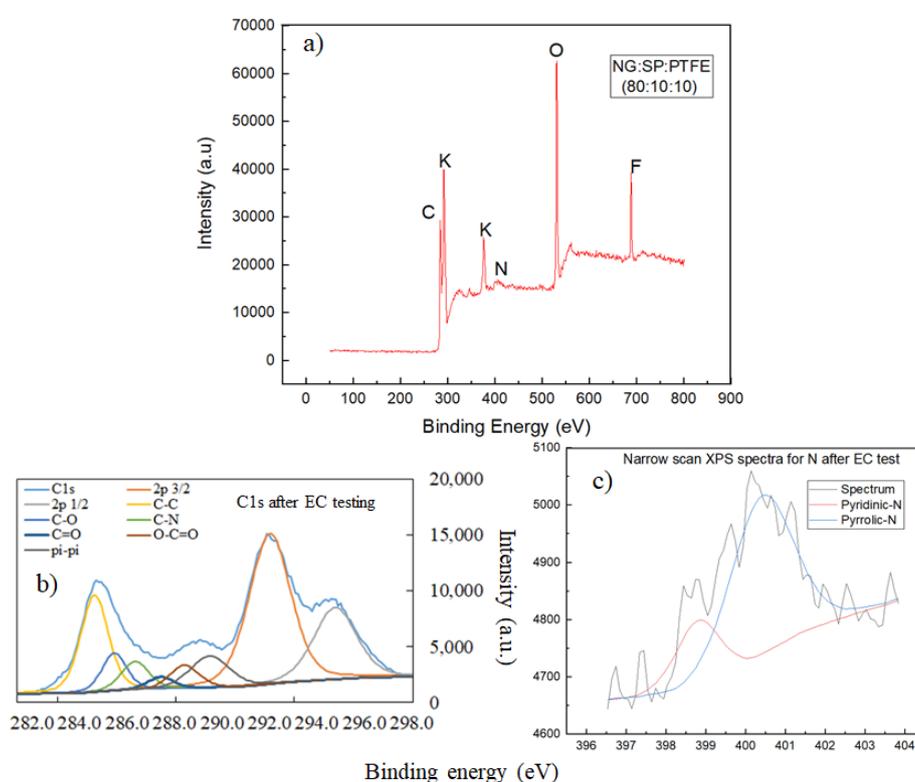

Figure 7. XPS analyses of the sample after electrochemical testing. a) Survey spectrum, b) narrow scan for C1s area, and c) narrow scan for N1s area.

Figure 8(a) shows the structure of the lattice before electrochemical test where 2 bonding configurations can be observed, which are pyridinic-N and pyrrolic-N. There is a presence of potassium in Figure 8(b) which comes from the KOH electrolyte and thus reduces the amount of the N in the lattice at pyridinic-N and pyrrolic-N bonds.
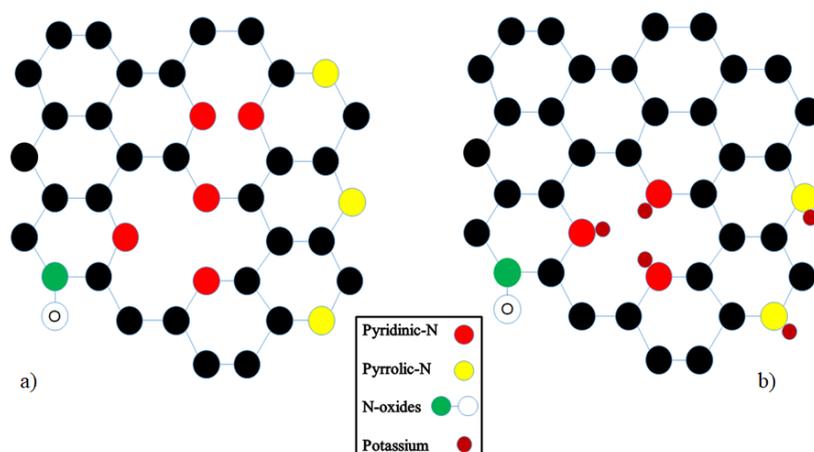
Figure 8. Suggested structure formation of N-doped graphene, a) before and b) after electrochemical testing.

4. CONCLUSION

The N-doped graphene has been successfully synthesized using hydrothermal method. From Raman analysis, the I_D/I_G ratio of of N-doped graphene has a higher value of than that of pristine graphene nanoplatelet. N-doped graphene has more defects and a higher degree of disorder compared to pristine graphene nanoplatelets. XRD analysis proved that there is formation of multiple layers of graphene after the process of doping nitrogen into graphene. XPS analysis proved that the percentage of atomic concentration of N into graphene is 2.35 %. The narrow scan of XPS shows existing common bonding configuration of N-doped graphene in the electrode which is pyridinic and pyrrolic. The electrochemical performance analyses revealed that this electrode has an ideal characteristic to work as supercapacitor and also produced a relatively good specific capacitance value. This indicates this electrode is suitable for the use in energy storage device. Future work may focus on the elaborated electrochemical testing like cyclic stability test to confirm the capacitance retention and also on the study of equivalent series resistance of the fabricated device.

REFERENCES

[1] S. Goswami, G. R. Dillip, S. Nandy, A. N. Banerjee, A. Pimentel, S. W. Joo, R. Martins, E. Fortunato, Electrochim. Acta., vol **316** (2019) pp. 202-218.
[2] Y. Kumar, S. Rawal, B. Joshi, S. A. Hashmi, J. Solid State Electrochem., vol **23**, no. 3 (2019) pp. 667-692.

[3] J. Feng, N. A. Chernova, F. Omenya, L. Tong, A. C. Rastogi, M. S. Whittingham, J. Solid State Electrochem., vol **22**, no. 4 (2018) pp. 1063-1078.

[4] M. A. Azam, N. Dorah, R. N. A. R. Seman, N. S. A. Manaf, T. I. T. Kudin, Mater. Technol., vol **30**, no. A1 (2015) pp. A14-A17.

[5] R. N. A. R. Seman, M. A. Azam, A. A. Mohamad, Renewable Sustainable Energy Rev., vol **75** (2017) pp. 644-659.

[6] H. Lu, et al., J. Mater. Sci. - Mater. Electron., vol **30**, no. 15 (2019) pp. 13933-13938.

[7] M. Teuber, M. Strautmann, J. Drillkens, D. U. Sauer, ACS Appl. Mater. Interfaces, vol **11**, no. 20 (2019) pp. 18313-18322.

[8] M. A. Azam, N. E. S. A. A. Mudtalib, R. N. A. R. Seman, Mater. Today Commun., vol **15** (2018) pp. 81-87.

[9] R. N. A. R. Seman, M. A. Azam, J. Sci.: Adv. Mater. Devices, vol **5**, no. 4 (2020) pp. 554-559.

[10] H. Gheybi, S. Sattari, K. Soleimani, M. Adeli, J. Iran. Chem. Soc., vol **17** (2020) pp. 735–764.

[11] M. A. Azam, et al., Diamond Relat. Mater., vol **104** (2020) pp. 107767.

[12] P. V. Bakharev, et al., Nat. Nanotechnol., vol **15**, no. 1 (2020) pp. 59-66.

[13] N. E. Safie, M. A. Azam, M. F. A. Aziz, M. Ismail, Int. J. Energy Res., vol **45**, no. 2 (2021) pp. 1347-1374.

[14] M. A. Azam, et al., ECS J. Solid State Science and Technology, vol **6**, no. 6 (2017) pp. M3035-M3048.

[15] L. H. Xu, et al., Nanoscale Res. Lett., vol **15** (2020) pp. 56.

[16] Y. Hu, et al., Carbon, vol **157** (2020) pp. 340-349.

[17] O. Sboychakov, A. V. Rozhkov, A. L. Rakhmanov, F. Nori, Phys. Rev. Lett., vol **120**, no. 26 (2018) pp. 266402.

[18] F. Ke, et al., Proc. Natl. Acad. Sci. USA, vol **116**, no. 19 (2019) pp. 9186-9190.

[19] M. Serry, M. A. Sakr, Sens. Actuators A, vol **245** (2016) pp. 169-179.

[20] S. Nigar, Z. Zhou, H. Wang, M. Imtiaz, RSC Adv., vol **7**, no. 81 (2017) pp. 51546-51580

[21] E. Ismail, et al., RSC Adv., vol **9**, no. 36 (2019) pp. 21000-21008.

[22] Adetayo, D. Runsewe, Open J. Composite Materials, vol **9**, no. 02 (2019) pp. 207.

[23] Z. Zhang, A. Fraser, S. Ye, G. Merle, J. Barralet, Nano Futures, vol **3**, no. 4 (2019) pp. 042003.

[24] E. Memarian, S. S. H. Davarani, S. Nojavan, S. K. Movahed, Anal. Chim. Acta, vol **935** (2016) pp. 151-160.

[25] Y. Wang, L. Yu, W. Zhu, X. Zhou, Y. Chen, W. Peng, Ionics, vol **25** (2019) pp. 3499–3522.

[26] M. A. A. Mohamed, N. A. Elessawy, F. Carrasco-Marín, H. A. Hamad, Phys. Chem. Chem. Phys., vol **21**, no. 25 (2019) pp. 13611-13622.

[27] S. Bhattacharyya, et al., Nat. Commun., vol **8**, no. 1 (2017) pp. 1-9.

[28] Y. Huang, D. D. Babu, Z. Peng, Y. Wang, Adv. Sci., vol **7**, no. 4 (2020) pp. 1902390.

[29] J. Zhang, et al., Sci. Rep., vol **6** (2016) pp. 28330.

[30] H. Miao, et al., Int. J. Hydrogen Energy, vol **42**, no. 47 (2017) pp. 28298-28308.

[31] K. K. Karuppanan, et al., Sustainable Energy Fuels, vol **3**, no. 4 (2019) pp. 996-1011.

[32] M. Ayiania, A. J. R. Hensley, K. Groden, M. Garcia-Perez, J. S. McEwen, Carbon, vol **152** (2019) pp. 715-726.

[33] G. Cárdenas-Jirón, Y. Figueroa, N. Kumar, J. M. Seminario, J. Phys. Chem. C, vol **120**, no. 4 (2016) pp. 2013-2026.

[34] M. Yu, et al., RSC Adv., vol **7**, no. 25 (2017) pp. 15293-15301.

[35] H. Liu, J. Zhang, B. Zhang, L. Shi, S. Tan, L. Huang, Electrochim. Acta., vol **138** (2014) pp. 69-78.

[36] Y. Wang, et al., Appl. Surf. Sci., vol **512** (2020) pp. 145711.

[37] B. Wang, V. Likodimos, A. J. Fielding, R. A. W. Dryfe, Carbon, vol **160** (2020) pp. 236-246.

[38] H. M. Jeong, et al., Nano letters, vol **11**, no. 6 (2011) pp. 2472-2477.

[39] M. A. Azam, K. Isomura, A. Fujiwara, T. Shimoda, Phys. Status Solidi A, vol **209**, no. 11 (2012) pp. 2260-2266.

[40] B. Deng, et al., Carbon, vol **138** (2018) pp. 169-178.

[41] N. M. S. Hidayah, W. W. Liu, C. S. Khe, C. W. Lai, N. Z. Noriman, U. Hashim, Mater. Today: Proc., vol **17** (2019) pp. 508-515.

[42] T. D. Thanh, N. D. Chuong, H. V. Hien, N. H. Kim, J. H. Lee, ACS Appl. Mater. Interfaces, vol **10**, no. 5 (2018) pp. 4672-4681.

[43] P. J. Yen, et al., Mater. Today Energy., vol **12** (2019) pp. 336-347.

[44] R. N. A. R. Seman, M. A. Azam, M. H. Ani, Nanotechnology, vol **29**, no. 50 (2018) pp. 502001.

[45] G. Chen, S. Tang, Y. Song, X. Meng, J. Yin, Y. Xia, Z. Liu, Chem. Eng. J., vol **361** (2019) pp. 387-397.

[46] R. Jaiswal, U. Saha, T. H. Goswami, A. Srivastava, N. E. Prasad, Electrochim. Acta, vol **283** (2018) pp. 269-290.

[47] S. Rey, F. Le Normand, Thin Solid Films, vol **519**, no. 14 (2011) pp. 4426-4428.

[48] N. Cao, G. Zheng, Nano Res., vol **11**, no. 6 (2018) pp. 2992-3008.